Molecular Astrophysics 1 (2015) 20–25

Contents lists available at ScienceDirect

Molecular Astrophysics

journal homepage: www.elsevier.com/locate/molap

High-resolution absorption cross sections of C_2H_6 at elevated temperatures

Robert J. Hargreaves*, Eric Buzan, Michael Dulick, Peter F. Bernath

Department of Chemistry, Old Dominion University, 4541 Hampton Boulevard, Norfolk, VA 23529, USA

ARTICLE INFO

Article history:
Received 11 August 2015
Revised 4 September 2015
Accepted 4 September 2015
Available online 19 October 2015

Keywords:
Giant planets
High temperatures
Exoplanets
Absorption cross sections
Infrared
High-resolution

ABSTRACT

Infrared absorption cross sections near 3.3 μm have been obtained for ethane, C_2H_6. These were acquired at elevated temperatures (up to 773 K) using a Fourier transform infrared spectrometer and tube furnace with a resolution of 0.005 cm^{-1}. The integrated absorption was calibrated using composite infrared spectra taken from the Pacific Northwest National Laboratory (PNNL). These new measurements are the first high-resolution infrared C_2H_6 cross sections at elevated temperatures.

1. Introduction

Ethane (C_2H_6) is the second largest component of natural gas and is primarily used in the industrial manufacture of petrochemicals. It is present as a trace gas in the Earth's atmosphere and can be used to monitor anthropogenic (e.g., fossil fuel emission, combustion processes) and biogenic sources (Aydin et al., 2011; Klingbeil et al., 2007; Tereszchuk et al., 2011).

However, C_2H_6 is also of particular interest to astronomy. C_2H_6 is found in all four giant planets (Hanel et al., 1981; Niemann et al., 2005; Orton et al., 1987; Ridgway, 1974), comets (Mumma et al., 1996) and even as an ice in Kuiper Belt objects (Brown et al., 2007). For Titan, observations indicate C_2H_6 is a constituent of light hydrocarbon lakes (Brown et al., 2008). In the atmospheres of the giant planets and Titan, C_2H_6 is primarily formed from the photolysis of methane, CH_4 (Mueller-Wodarg et al., 2008; Nixon et al., 2007), and subsequent recombination of methyl radicals, CH_3 (Krasnopolsky, 2009, 2014; Wilson and Atreya, 2009).

In Jupiter, stratospheric observations have detected hot C_2H_6 in polar auroral regions (Kim et al., 2009). These hot spots occur close to similar hot CH_4 and H_3^+ emission (Kim et al., 2015) and are heated due to the channeling of particles by the strong magnetic field. The Juno mission (Matousek, 2007) is due to arrive at Jupiter in 2016 and one major objective for the Jovian Infrared Auroral Mapper, JIRAM (Adriani et al., 2008), is to study these auroral hot spots to determine the molecules responsible and their vertical structure.

Brown dwarfs are sub-stellar objects that do not burn hydrogen in their cores (Kirkpatrick, 2005). They are warm (albeit relatively cool in comparison to stars), thereby allowing for the formation of rich molecular atmospheres. Brown dwarf atmospheric chemical models predict C_2H_6 to form deep in these objects (Lodders and Fegley, 2002). Recent observations indicate that these objects can also harbour extremely bright aurorae (Hallinan et al., 2015). Similarly, exoplanets known as hot-Jupiters orbit close to their parent star and have atmospheric temperatures conducive to molecule formation. While models predict C_2H_6 may have a low thermochemical abundance in the atmosphere of these objects (Venot et al., 2012), disequilibrium and increased metallicity can lead to significant enhancements (Bilger et al., 2013; Line et al., 2011; Moses et al., 2011). C_2H_6 can be used as a useful temperature probe for exoplanets and brown dwarfs (Tinetti et al., 2013), but high temperature laboratory data are missing. It is therefore important to have high temperature data available for astronomical and terrestrial applications.

Due to the prevalence of C_2H_6, the infrared spectrum has been the focus of numerous studies, but complete line assignments are difficult to obtain. This is, in part, due to the ν_4 torsional mode near 35 μm (290 cm^{-1}) (Borvayeh et al., 2008; Moazzen-Ahmadi et al., 2001, 2015, 1999) which produces numerous low frequency hot bands, extensive perturbations and a very dense line structure. The ν_9 mode near 12 μm (830 cm^{-1}), often used in remote sensing (von Clarmann et al., 2007; Vinatier et al., 2015), has been the focus of comprehensive analyses that have significantly improved line

* Corresponding author.
E-mail address: rhargrea@odu.edu (R.J. Hargreaves).

http://dx.doi.org/10.1016/j.molap.2015.09.001
2405-6758/

Table 1
Experimental conditions and Fourier transform parameters.

Parameter	Value[a]
Temperature range	296 – 773 K
Spectral range	2200 – 5600 cm^{-1}
Resolution	0.005 cm^{-1}
Path length	0.5 m
Sample cell material	Quartz (SiO_2)
External source	External globar[b]
Detector	Indium antimonide (InSb)
Beam splitter	Calcium fluoride (CaF_2)
Spectrometer windows	CaF_2
Filter	Germanium
Aperture	1.5 mm
Apodization function	Norton-Beer, weak
Phase correction	Mertz
Zero-fill factor	× 16

[a] all spectra recorded under same conditions except where stated.
[b] no external source for B_{em} and B_{ref}.

assignments (Malathy Devi et al., 2010a, 2010b, Vander Auwera et al., 2007). Line parameters and assignments have been obtained for the ν_8 band near 6.8 μm (1470 cm^{-1}) (di Lauro et al., 2012; Lattanzi et al., 2011a; 2008) as well as the ν_5 and ν_7 modes contained in the 3.3 μm (3000 cm^{-1}) spectral region (Lattanzi et al., 2011b; Villanueva et al., 2011). Although considerable progress has been made in these recent studies, high-resolution analyses are generally incomplete and still fail to match laboratory observations precisely.

The Pacific Northwest National Laboratory (PNNL) has recorded infrared absorption cross sections for a large number of species, including C_2H_6 (see http://nwir.pnl.gov and Sharpe et al., 2004), at three temperatures (278, 293 and 323 K). High-resolution (0.004 cm^{-1}) absorption cross sections have been provided at room temperature (Harrison et al., 2010) and these measurements constitute the C_2H_6 cross sections contained in HITRAN (Rothman et al., 2013). However, the intended use of these data are for the study of the Earth's atmosphere and will give an incorrect radiative transfer when applied to high temperature environments. High-temperature absorption cross sections of hydrocarbon species (including C_2H_6) have been recorded for combustion applications (Alrefae et al., 2014) at relatively low resolution (≥ 0.16 cm^{-1}) and are not sufficient for high-resolution applications.

The aim of this work is to provide high-resolution absorption cross sections of C_2H_6 at elevated temperatures to be used in the analysis of brown dwarfs, exoplanets and auroral hot spots of Jupiter.

2. Measurements

Spectra were acquired of C_2H_6 between 2200 and 5600 cm^{-1} (1.8 – 4.5 μm) using a Fourier transform infrared spectrometer at a resolution of 0.005 cm^{-1}. These spectra cover the temperatures 296 – 773 K and experimental conditions are provided in Table 1.

The spectrometer is combined with a tube furnace containing a sample cell made entirely from quartz, thereby allowing the cell to be contained completely within the heated portion of the furnace (Hargreaves et al., 2015b). At elevated temperatures, the C_2H_6 infrared spectrum has both emission and absorption components. The emission components can be included in the final transmittance spectra by following the same procedure outlined in Hargreaves et al. (2015b) for CH_4. This involves recording both C_2H_6 absorption (A_{ab}) and emission (B_{em}) spectra, then combining as

$$\tau = \frac{A_{ab} - B_{em}}{A_{ref} - B_{ref}}, \quad (1)$$

to give the transmittance spectrum (τ), where A_{ref} and B_{ref} are the background reference spectra of the absorption and emission, respectively. The emission component of C_2H_6 is sufficiently strong at 673 and 773 K that an emission correction is necessary; therefore B_{em} and B_{ref} are required. For lower temperatures, B_{em} and B_{ref} equal zero and Eq. 1 reverts to the standard transmittance equation (i.e., $\tau = A_{ab}/A_{ref}$).

Table 2
Summary of C_2H_6 measurements.

Mode	Sample temperature (K)	Sample C_2H_6 pressure (Torr)	Sample scans	Background scans
Absorption	297	0.276	400	550
	297	0.035	24	24
	473	0.982	300	300
	473	0.176	24	24
	573	1.476	300	300
	573	0.282	24	24
	673	2.928	150	150
	673	0.987	24	24
	773	5.026	150	150
	773	1.557	24	24
Emission	673	3.067	150	150
	673	1.008	24	24
	773	5.206	150	150
	773	1.534	24	24

The C_2H_6 infrared spectrum near 3000 cm^{-1} (3.3 μm) contains a small number of ν_7 *Q*-branch features that are significantly stronger than the *P*- and *R*-branches and the nearby ν_5 mode. In order to maximize the signal from the weaker features, the C_2H_6 spectra were acquired at both "high" and "low" pressure. These high and low pressure experiments are summarised in Table 2. The low pressure spectra were recorded to determine the absorption cross sections of these strong *Q*-branch features. These *Q*-branch cross sections were then added to the high pressure absorption cross sections in place of the high pressure *Q*-branch features, which had been intentionally saturated (see Section 3).

3. Absorption cross sections

An absorption cross section, σ (cm^2 $molecule^{-1}$), can be calculated using

$$\sigma = -\xi \frac{10^4 k_B T}{Pl} \ln \tau, \quad (2)$$

where T is the temperature (K), P is the pressure of the absorbing gas (Pa), l is the optical pathlength (m), τ is the observed transmittance spectrum, k_B is the Boltzmann constant and ξ is a normalization factor (Hargreaves et al., 2015a; Harrison et al., 2010).

It has been demonstrated by numerous studies on a variety of molecular spectra that integrating an absorption cross section over an isolated band (containing primarily fundamentals) exhibits an insignificant temperature dependence (Breeze et al., 1965; Crawford, 1958; Harrison et al., 2010; 2012; Harrison and Bernath, 2010; Mills and Whiffen, 1959; Yao and Overend, 1976).

The PNNL infrared absorption cross sections of C_2H_6 cover the spectral range 600–6500 cm^{-1} (resolution of 0.112 cm^{-1}) at 278, 293

Table 3
Parameters for calibrated absorption cross sections.

Temperature (K)	Normalization factor ξ	C_2H_6 effective pressure (Torr)	Integrated absorption cross section (×10^{-17} cm $molecule^{-1}$)
297	1.028	0.269	2.978
473	1.035	0.948	2.978
573	1.063	1.388	2.976
673	1.047	2.796	2.975
773	1.033	4.867	2.976

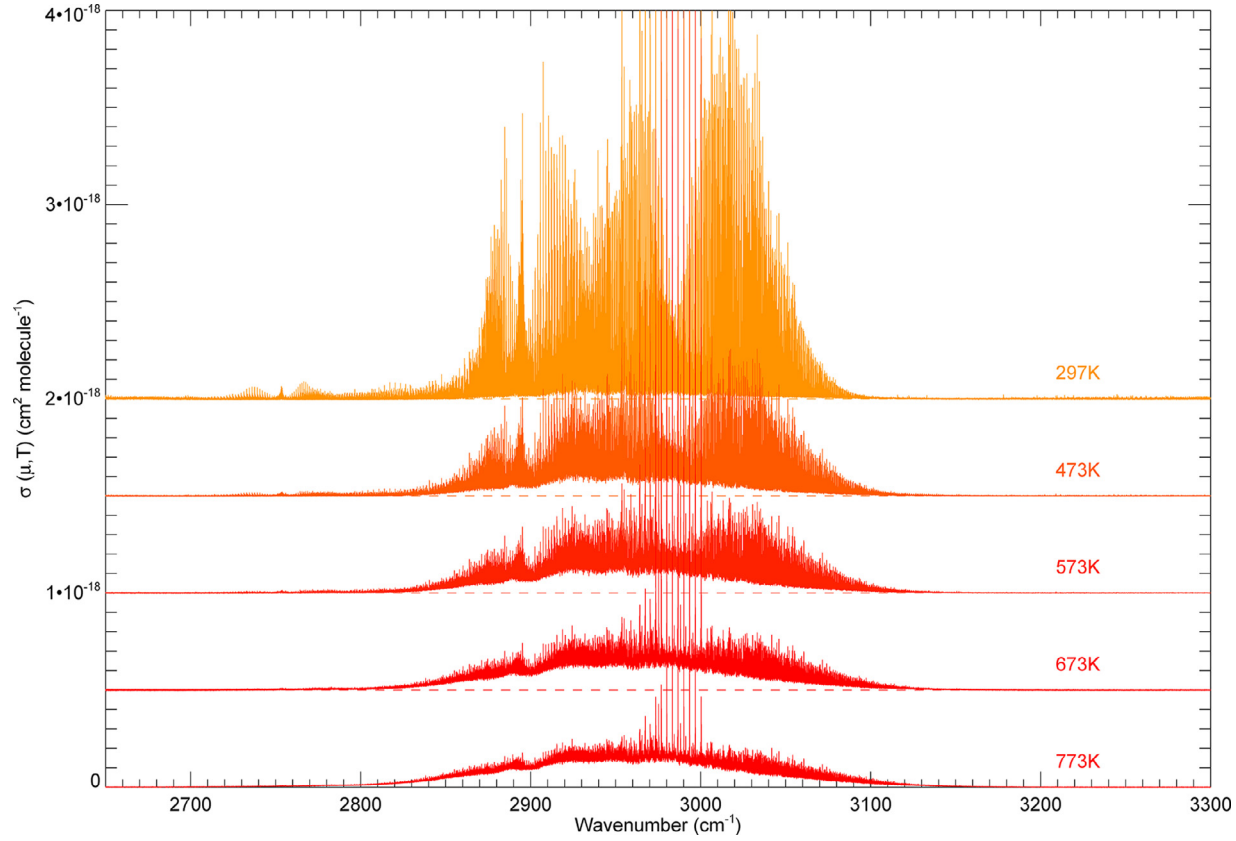

Fig. 1. C_2H_6 cross sections of the 3.3 μm region at elevated temperatures. Due to the strength of the ν_7 Q-branches, each temperature has been offset by 5×10^{-19} cm^2 molecule^{-1} to highlight the detail in the surrounding region. The baseline for each temperature is given by the corresponding dashed line (For interpretation of the references to colour in this figure legend, the reader is referred to the web version of this article).

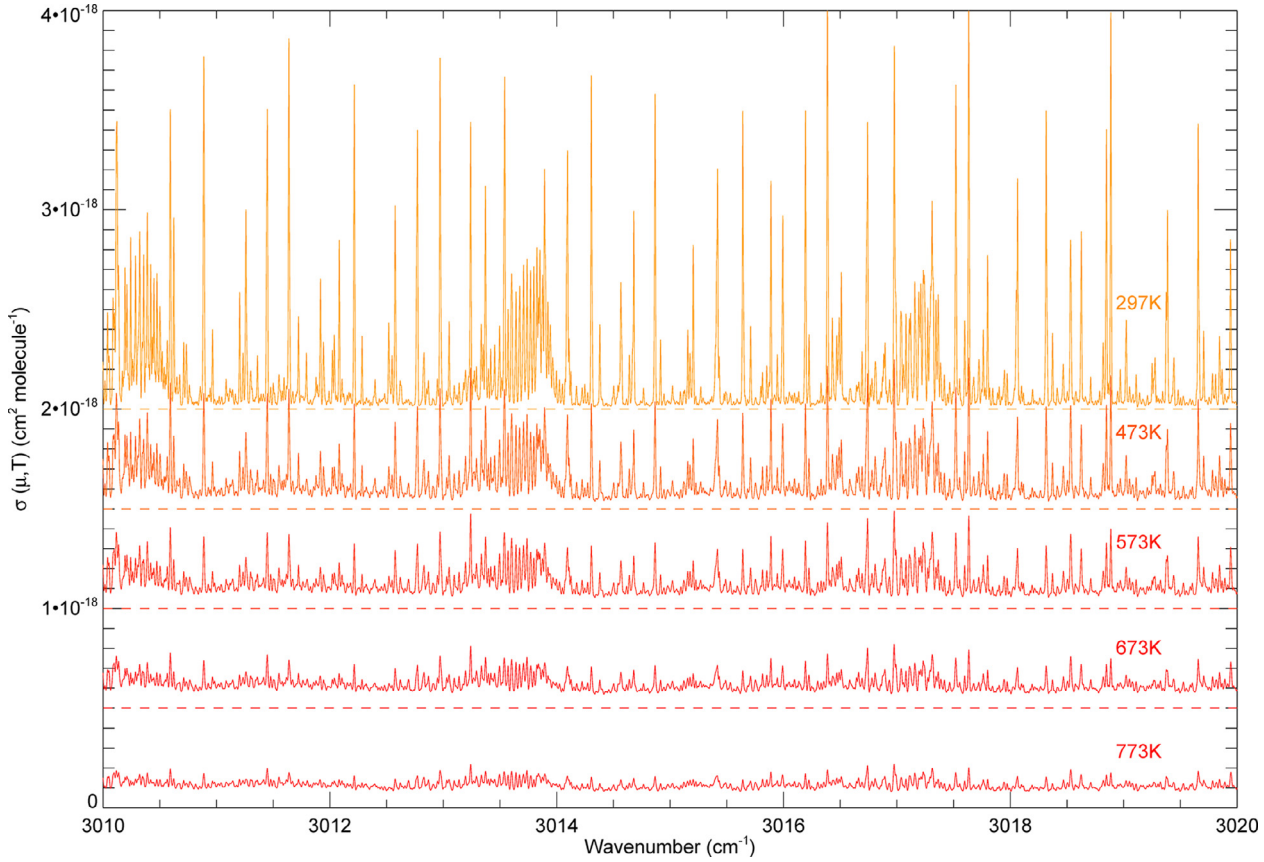

Fig. 2. C_2H_6 cross sections in the vicinity of the $^rQ_7$ (3010.7 cm^{-1}), $^rQ_8$ (3014.0 cm^{-1}) and $^rQ_9$ (3017.5 cm^{-1}) branches of the ν_7 mode. The baseline for each temperature is given by the corresponding dashed line (For interpretation of the references to colour in this figure legend, the reader is referred to the web version of this article).

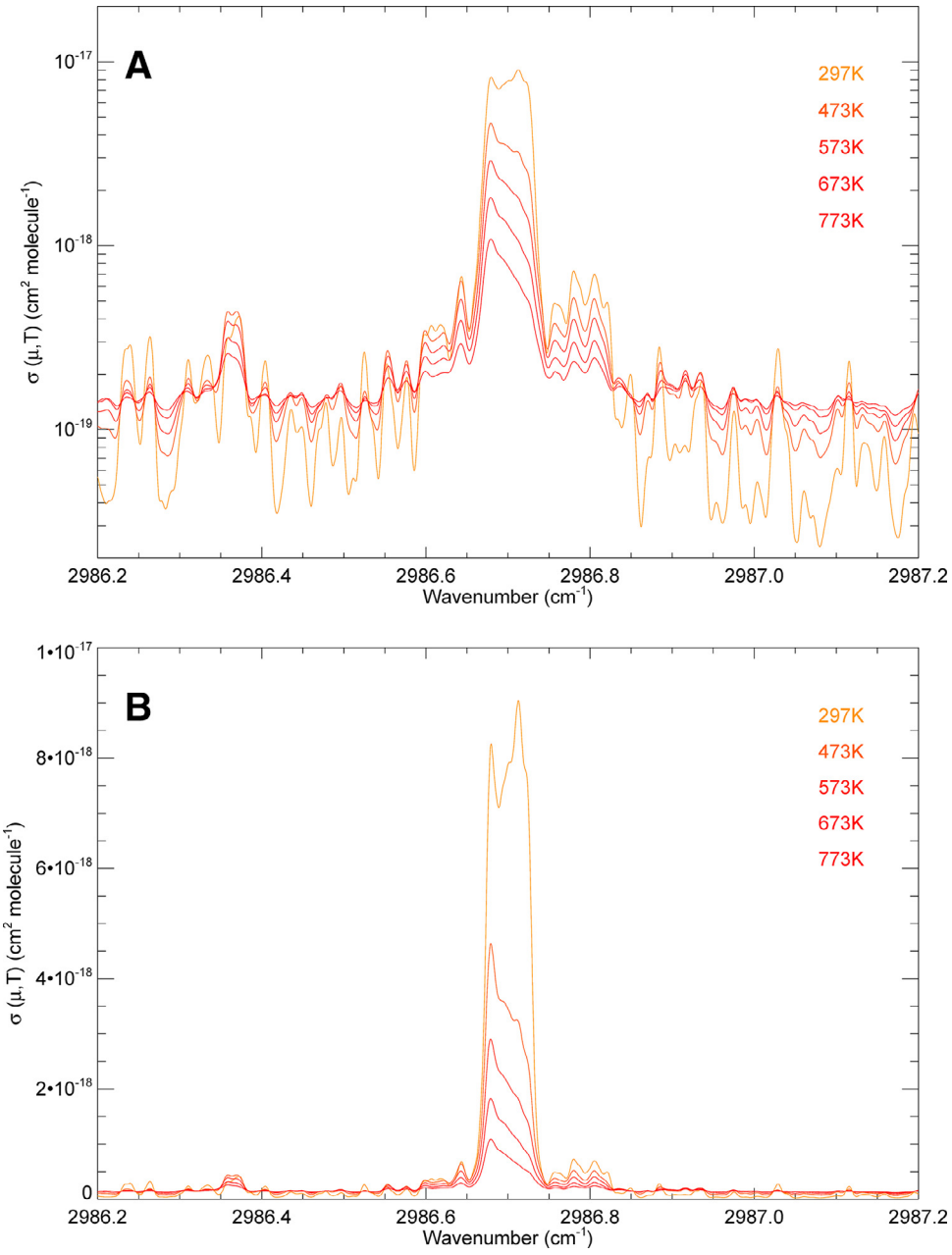

Fig. 3. Temperature dependance of the $^{r}Q_0$-branch of the ν_7 mode of C_2H_6. (A) The decreasing $^{r}Q_0$-branch is observed as the surrounding continuum increases, using a logarithmic scale. (B) The shape of the $^{r}Q_0$-branch is seen to change shape at higher temperatures on a linear scale (For interpretation of the references to colour in this figure legend, the reader is referred to the web version of this article).

and 323 K. Each PNNL cross section is a composite of approximately ten pathlength concentrations, making these data suitably accurate for calibration (Harrison et al., 2010). For the spectral region between 2500 and 3500 cm^{-1} the average PNNL integrated absorption is calculated as

$$\int_{2500\ cm^{-1}}^{3500\ cm^{-1}} \sigma(\nu, T)d\nu = 2.976(\pm 0.011) \times 10^{-17}\ \text{cm molecule}^{-1}. \quad (3)$$

Each individual PNNL cross section demonstrates less than 0.4% deviation from this value[1].

The new transmittance spectra have been converted into cross sections using Eq. 3, making the original assumption that $\xi = 1$. This is to allow the strong ν_7 Q-branch features from the low pressure observations to be inserted in place of the same saturated (therefore distorted) Q-branch features in the high pressure absorption cross sections. Each replaced Q-branch region covered less than $\sim$ 0.2 cm^{-1} and was chosen to be between the points where the high and low pressure cross sections intersect either side of the strong feature. These composite absorption cross sections were then integrated over the 2500 and 3500 cm^{-1} spectral region. Comparisons were made to the PNNL integrated absorption cross section (Eq. 3) in order to calibrate our observations. The normalization factors for each absorption cross section are provided in Table 3, alongside the calibrated pressures and calibrated integrated absorption cross sections.

[1] PNNL units ($ppm^{-1}m^{-1}$ at 296 K) have been converted using the factor $k_B \times 296 \times \ln(10) \times 10^4/0.101325 = 9.28697 \times 10^{-16}$ (Harrison et al., 2012)

The calibrated cross sections are displayed in Fig. 1 between 2600 and 3300 cm^{-1} and clearly display the ν_5 and ν_7 fundamental bands. Fig. 2 shows a 10 cm^{-1} section of Fig. 1 in the vicinity of three weak ν_7 *Q*-branch features; an increase in the observed continuum at higher temperatures can be seen.

The calibrated absorption cross sections described in Table 3 are available online[2] in the standard HITRAN format (Rothman et al., 2013).

4. Discussion

The normalization factors are necessary to account for the difficulty in measuring the experimental parameters accurately (i.e., pathlength, pressure and temperature). The combination of the errors often leads to an underestimation of the integrated absorption cross section, which is calibrated by comparison to the PNNL data. Normalization factors are typically within 6% for measurements using similar apparatus (e.g., Harrison et al., 2010). For our measurements, the normalization factor has been used to give an effective calibrated pressure as seen in Table 3. Based upon consideration of the experimental and photometric errors, the calibrated cross sections are expected to be accurate to within 4%.

The C_2H_6 absorption cross sections available at 194 K are also based on a calibration to PNNL (Harrison et al., 2010). These data contains C_2H_6 at 0.2208 Torr, which has been broadened by 103.86 Torr of air at a resolution of 0.015 cm^{-1}. Integrating the available data between 2545 and 3315 cm^{-1} yields a value of 2.985×10^{-17} cm $molecule^{-1}$. This is within 0.3% of the average values contained in Table 3. An independent quality check can be made by comparing to new C_2H_6 absorption cross sections recorded for combustion applications (Alrefae et al., 2014). These data contain medium resolution (0.16–0.6 cm^{-1}) nitrogen-broadened cross sections of C_2H_6 between 2500 and 3400 cm^{-1}. At temperatures of 296, 673 and 773 K the C_2H_6 integrated absorption cross sections were calculated to be 2.81×10^{-17}, 2.99×10^{-17} and 3.08×10^{-17} cm $molecule^{-1}$, respectively. While a small temperature dependence is seen when compared to our values in Table 3, the deviation is within their experimental error (5%).

Experimental spectra of C_2H_6 have not been acquired at temperatures above 773 K as the molecules begin to decompose when using a sealed cell. Evidence of CH_4 absorption was observed at 873 K; therefore reliable C_2H_6 cross sections could not be obtained.

C_2H_6 is expected to be useful as a temperature probe for exoplanets and brown dwarfs (Tinetti et al., 2013). The infrared spectrum (Figs. 1 and 2) demonstrates a continuum-like feature previously observed for CH_4 at high temperatures (Hargreaves et al., 2015b). It can be seen that as the continuum increases with temperature, the sharp *Q*-branches decrease due to a change in the population of states and they also broaden because of the increasing Doppler width (Fig. 3). However, Table 3 shows ξ only exhibits a small change and the integrated intensity remains constant (within experimental error). This variation is small enough to justify the assumption that the integrated absorption cross sections are independent of temperature.

For weak concentrations of C_2H_6 it may be difficult to observe a change in the continuum, particularly since the 3.3 μm region contains the prominent C-H stretch for hydrocarbons. However, the shape of the sharp *Q*-branches of the ν_7 mode are also seen to change with increasing temperature, as shown in Fig. 3. These *Q*-branches are relatively easy to identify in congested atmospheric spectra, therefore studying the shape of these features can also be used to infer temperatures.

[2] http://bernath.uwaterloo.ca/C2H6/

5. Conclusion

High-resolution infrared absorption cross sections for C_2H_6 have been measured at elevated temperatures (up to 773 K) between 2500 and 3500 cm^{-1}. The spectra were recorded at a resolution of 0.005 cm^{-1} and the integrated absorption has been calibrated to PNNL values. These data are of particular interest for simulating astronomical environments at elevated temperatures, such as brown dwarfs and exoplanet atmospheres, where C_2H_6 can be used as a temperature probe. With the imminent arrival of the Juno spacecraft into orbit around Jupiter, these data will be of particular use for observations made of aurora using the JIRAM instrument.

Acknowledgments

Funding was provided by the NASA Outer Planets Research Program.

References

Adriani, A., Coradini, A., Filacchione, G., et al. 2008, Astrobiology, 8, 613–622. doi:10.1089/ast.2007.0167.
Alrefae, M., Es-sebbar, E.-t., & Farooq, A. 2014, J. Mol. Spectrosc., 303, 8–14. doi:10.1016/j.jms.2014.06.007.
Aydin, M., Verhulst, K.R., Saltzman, E.S., et al. 2011, Nature, 476, 198–201. doi:10.1038/nature10352.
Bilger, C., Rimmer, P., & Helling, C. 2013, Mon. Notices R. Astronom. Soc., 435, 1888–1903. doi:10.1093/mnras/stt1378. arXiv: 1307.2565.
Borvayeh, L., Moazzen-Ahmadi, N., & Horneman, V.-M. 2008, J. Mol. Spectrosc., 250, 51–56. doi:10.1016/j.jms.2008.04.009.
Breeze, J.C., Ferriso, C.C., Ludwig, C.B., & Malkmus, W. 1965, J. Chem. Phys., 42, 402–406. doi:10.1063/1.1695707.
Brown, M.E., Barkume, K.M., Blake, G.A., Schaller, E.L., et al. 2007, Astron. J., 133, 284–289. doi:10.1086/509734.
Brown, R.H., Soderblom, L.A., Soderblom, J.M., et al. 2008, Nature, 454, 607–610. doi:10.1038/nature07100.
von Clarmann, T., Glatthor, N., Koukouli, M.E., et al. 2007, Atmosph. Chem. Phys., 7, 5861–5872. doi:10.5194/acp-7-5861-2007.
Crawford Jr., B. 1958, J. Chem. Phys., 29, 1042–1045. doi:10.1063/1.1744652.
di Lauro, C., Lattanzi, F., Brown, L.R., et al. 2012, Planet. Space Sci., 60, 93–101. doi:10.1016/j.pss.2011.01.008.
Hallinan, G., Littlefair, S.P., Cotter, G., et al. 2015, Nature, 523, 568–571. doi:10.1038/nature14619.
Hanel, R., Conrath, B., Flasar, F.M., et al. 1981, Science, 212, 192–200. doi:10.1126/science.212.4491.192.
Hargreaves, R.J., Bernath, P.F., & Appadoo, D.R.T. 2015a, J. Mol. Spectrosc., 315, 102–106. doi:10.1016/j.jms.2015.03.014.
Hargreaves, R.J., Bernath, P.F., Bailey, J., & Dulick, M. 2015b, Astrophys. J. in press.
Harrison, J.J., Allen, N.D.C., & Bernath, P.F. 2010, J. Quant. Spectrosc. Radiat. Transfer, 111, 357–363. doi:10.1016/j.jqsrt.2009.09.010.
Harrison, J.J., Allen, N.D.C., & Bernath, P.F. 2012, J. Quant. Spectrosc. Radiat. Transfer, 113, 2189–2196. doi:10.1016/j.jqsrt.2012.07.021.
Harrison, J.J. & Bernath, P.F. 2010, J. Quant. Spectrosc. Radiat. Transfer, 111, 1282–1288. doi:10.1016/j.jqsrt.2009.11.027.
Kim, S.J., Geballe, T.R., Seo, H.J., & Kim, J.H. 2009, Icarus, 202, 354–357. doi:10.1016/j.icarus.2009.03.020.
Kim, S.J., Sim, C.K., Ho, J., et al. 2015, Icarus, 257, 217–220. doi:10.1016/j.icarus.2015.05.008.
Kirkpatrick, J.D. 2005, Annu. Rev. Astron. Astrophys., 43, 195–245. doi:10.1146/annurev.astro.42.053102.134017.
Klingbeil, A.E., Jeffries, J.B., & Hanson, R.K. 2007, J. Quant. Spectrosc. Radiat. Transfer, 107, 407–420. doi:10.1016/j.jqsrt.2007.03.004.
Krasnopolsky, V.A. 2009, Icarus, 201, 226–256. doi:10.1016/j.icarus.2008.12.038.
Krasnopolsky, V.A. 2014, Icarus, 236, 83–91. doi:10.1016/j.icarus.2014.03.041.
Lattanzi, F., di Lauro, C., & Auwera, J.V. 2011a, Mol. Phys., 109, 2219–2235. doi:10.1080/00268976.2011.604353.
Lattanzi, F., di Lauro, C., & Vander Auwera, J. 2011b, J. Mol. Spectrosc., 267, 71–79. doi:10.1016/j.jms.2011.02.003.
Lattanzi, F., Lauro, C.d., & Vander Auwera, J. 2008, J. Mol. Spectrosc., 248, 134–145. doi:10.1016/j.jms.2007.12.006.
Line, M.R., Vasisht, G., Chen, P., Angerhausen, D., & Yung, Y.L. 2011, Astronom. J., 738, 32. doi:10.1088/0004-637X/738/1/32. arXiv: 1104.3183.
Lodders, K. & Fegley, B. 2002, Icarus, 155, 393–424. doi:10.1006/icar.2001.6740.
Malathy Devi, V., Benner, D.C., Rinsland, C.P., et al. 2010, J. Quant. Spectrosc. Radiat. Transfer, 111, 2481–2504. doi:10.1016/j.jqsrt.2010.07.010.
Malathy Devi, V., Rinsland, C.P., Chris Benner, D., Sams, R.L., & Blake, T.A. 2010b, J. Quant. Spectrosc. Radiat. Transfer, 111, 1234–1251. doi:10.1016/j.jqsrt.2009.10.017.
Matousek, S. 2007, Acta Astron., 61, 932–939. doi:10.1016/j.actaastro.2006.12.013.
Mills, I.M. & Whiffen, D.H. 1959, J. Chem. Phys., 30, 1619–1620. doi:10.1063/1.1730254.

Moazzen-Ahmadi, N., Kelly, E., Schroderus, J., & Horneman, V.-M. 2001, J. Mol. Spectrosc., 209, 228–232. doi:10.1006/jmsp.2001.8427.
Moazzen-Ahmadi, N., Norooz Oliaee, J., Ozier, I., et al. 2015, J. Quant. Spectrosc. Radiat. Transfer, 151, 123–132. doi:10.1016/j.jqsrt.2014.09.016.
Moazzen-Ahmadi, N., Schroderus, J., & McKellar, A.R.W. 1999, J. Chem. Phys., 111, 9609–9617. doi:10.1063/1.480294.
Moses, J.I., Visscher, C., Fortney, J.J., et al. 2011, Astronom. J., 737, 15. doi:10.1088/0004-637X/737/1/15. arXiv: 1102.0063.
Mueller-Wodarg, I.C.F., Strobel, D.F., Moses, J.I., et al. 2008, Space Sci. Rev., 139, 191–234. doi:10.1007/s11214-008-9404-6.
Mumma, M.J., Disanti, M.A., dello Russo, N., et al. 1996, Science, 272, 1310–1314. doi:10.1126/science.272.5266.1310.
Niemann, H.B., Atreya, S.K., Bauer, S.J., et al. 2005, Nature, 438, 779–784. doi:10.1038/nature04122.
Nixon, C.A., Achterberg, R.K., Conrath, B.J., et al. 2007, Icarus, 188, 47–71. doi:10.1016/j.icarus.2006.11.016.
Orton, G.S., Aitken, D.K., Smith, C., et al. 1987, Icarus, 70, 1–12. doi:10.1016/0019-1035(87)90070-4.
Ridgway, S.T. 1974, Astrophys. J. Lett., 187, L41–L43. doi:10.1086/181388.
Rothman, L.S., Gordon, I.E., Babikov, Y., et al. 2013, J. Quant. Spectrosc. Radiat. Transfer, 130, 4–50. doi:10.1016/j.jqsrt.2013.07.002.
Sharpe, S.W., Johnson, T.J., Sams, R.L., et al. 2004, Appl. Spectrosc., 58, 1452–1461. doi:10.1366/0003702042641281.
Tereszchuk, K.A., González Abad, G., Clerbaux, C., et al. 2011, Atmos. Chem. Phys., 11, 12169–12179. doi:10.5194/acp-11-12169-2011.
Tinetti, G., Encrenaz, T., & Coustenis, A. 2013, Astron. Astrophys. Rev., 21, 63. doi:10.1007/s00159-013-0063-6.
Vander Auwera, J., Moazzen-Ahmadi, N., & Flaud, J.-M. 2007, Astrophys. J., 662, 750–757. doi:10.1086/515567.
Venot, O., Hébrard, E., Agúndez, M., et al. 2012, Astron. Astrophys., 546, A43. doi:10.1051/0004-6361/201219310. arXiv: 1208.0560.
Villanueva, G.L., Mumma, M.J., & Magee-Sauer, K. 2011, J. Geophys. Res. (Planets), 116, 8012. doi:10.1029/2010JE003794.
Vinatier, S., Bézard, B., Lebonnois, S., et al. 2015, Icarus, 250, 95–115. doi:10.1016/j.icarus.2014.11.019.
Wilson, E.H. & Atreya, S.K. 2009, J. Phys. Chem. A, 113, 11221–11226. doi:10.1021/jp905535a.
Yao, S.J. & Overend, J. 1976, Spectrochim. Acta Part A: Mol. Spectrosc., 32, 1059–1065. doi:10.1016/0584-8539(76)80290-5.